Arab J. Nucl. Sci. Appl., Vol. 55, 4, 92-108 (2022)

ISSN 1110-0451

Arab Journal of Nuclear Sciences and Applications

Web site: ajnsa.journals.ekb.eg

(E S N S A)

Radioelements Potentiality around Gabel Nugrus Area, South Eastern Desert, Egypt: Geological and Mineralogical Implications

Ibrahim A. Salem[1], Gehad M. Saleh[2], Mohamed S. Kamar[2], Ahmed R. Hamad[2*] and Mohamed Abd El Monsef[1].

[(1)] Geology Department, Faculty of Science, Tanta University Tanta, Egypt.

[(2)] Nuclear Materials Authority, Cairo, Egypt.

ARTICLE INFO

Article history:

Received: 10th Mar. 2022

Accepted: 4th Aug. 2022

Keywords:

Gabel Nugrus,
mineralogy,
uranium,
radioactivity,
spectrometric prospecting,
south Eastern Desert,
Egypt.

ABSTRACT

The present study spotlights on the geological, petrographical, mineralogical and radiometric prospecting, which control the distribution of radioactive elements within the granitic rocks of Gabel Nugrus. The study area is composed of ultramafic rocks, ophiolitic metagabbros, biotite hornblende gneisses and granitic rocks. The granitic rocks are represented by monzogranite, syenogranite and garnetiferous muscovite granite. The minerals (uranophane, uranothorite, fergusonite, zircon, monazite, xenotime, allanite, sphalerite, gold, arsenopyrite and pyrite) were identified by Scanning Electron Microscope (SEM) and back-scattered electron imaging system. In monzogranite, the average eU and eTh contents in both north and south of Gabel Nugrus are 9.25ppm, 5.4ppm, 31.41ppm, 19.29ppm respectively. In the syenogranite, the average eU, eTh contents are 10.22ppm and 24.45ppm respectively. In the garnetiferous muscovite granite, the average eU and eTh contents are 7.82ppm and 13.33ppm respectively. The radioactive anomaly in the study area is confined to the fractures cutting through the garnetiferous muscovite granite at the northern part of Gabel Magal El Harami area. The average of eU, eTh and eUm contents within fractures are187.87ppm, 109.57ppm, 156.57, this reflects a strong addition of uranium from the surrounding rocks. While the radioelements have been dissolved from the surrounding rocks (different types of granites) by meteoric and/or surface water through joints and fissures and finally, it deposited/trapped along the fractures of garnetiferous muscovite granites (absorbed by iron oxides) and less impermeable mica lenses due to the change in the physicochemical conditions, Eh and Ph in the given medium.

1. INTRODUCTION

The basement complex of the Eastern Desert of Egypt is subdivided into three domains (North Eastern Desert, Central Eastern Desert and South Eastern Desert) based on the dominating lithology and tectonic styles [1; 2].

Gabel (G.) Nugrus is bounded by three major faults, which separate G. Nugrus from the surrounding blocks; the first one runs into NW-SE nearly parallel to the Red Sea coast through Wadi (W.) Nugrus, while the second fault extends nearly NNW-SSE through W. El-Nom. The third major fault trends WNW-ESE to NW-SE direction. The first two faults are recognized as sinistral strike-slip faults, while the third one is a thrust fault [3]. G. Nugrus pluton forms an oval-shaped mass stretched in the NW-SE direction for about 16 km length and 8 Km width (Fig. 1a) and is characterized by moderate to highly rugged topographic terrains including conspicuous peak (Fig. 1b).

G. Nugrus granite is surrounded by medium to high-grade (Hafafit and Zabara gneisses) and low-grade metamorphic assemblage comprising ophiolitic rocks and island arc metavolcanics. It is separated from G. Hafafit by a strike-slip fault trending NW-SE and dipping 20°-50°NE. The fault is marked by a shear zone up to 600 m wide. Radioactive anomalies hosted in the granitic rocks are recorded in high values elsewhere in the Eastern Desert of Egypt, e.g. G. Gattar, [4-10].

The aim of the present work isto throw lights on the geological, petrographical, mineralogical features, which control the distribution of uranium and thorium within the granitic rocks through radiometric measurements.

Corresponding author: hmad801@yahoo.com

DOI: 10.21608/ajnsa.2022.126488.1560.

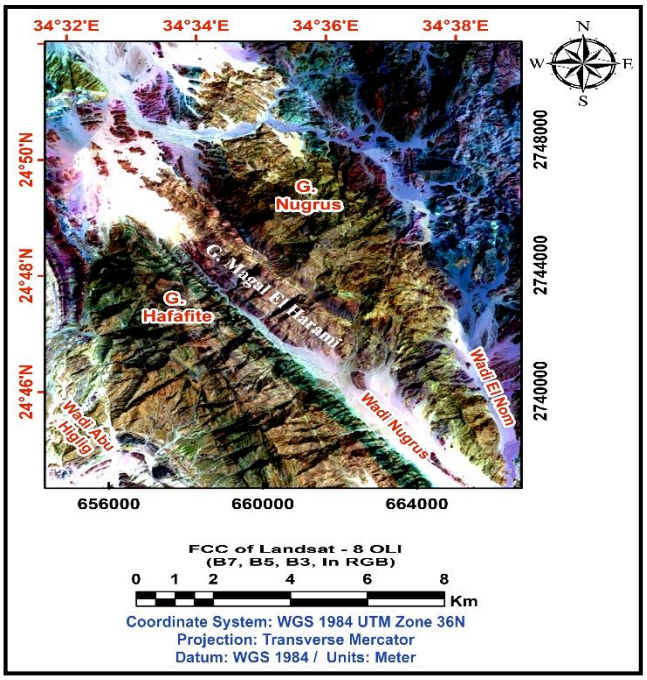

Fig. (1a): False color composite Landsat 8 image bands 7,5,3 in RGB,at G. Nugrus area, SED, Egypt.

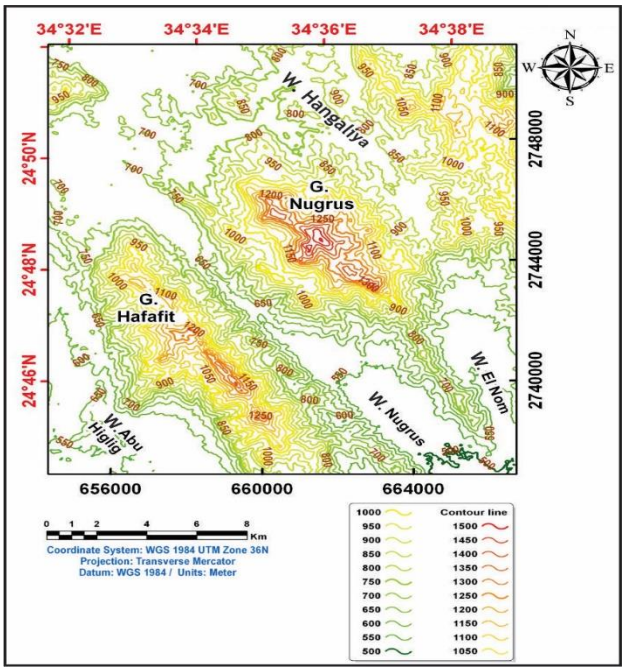

Fig. (1b): Contour topographic map of G. Nugrus area, SED, Egypt. (Derived from digital elevation model (DEM) with 12.5 m resolution).

2. GEOLOGICAL SETTING

G. Nugrus lies in the southern part of the Eastern Desert of Egypt at 60 km southwest of Marsa Alam City (Fig. 2a) and constitutes a part of the Arabian-Nubian shield. It is located between latitudes 24º 45` 00`` and 24º 52` 20`` N and longitudes 34º 29` 00`` and 34º 39` 20`` E (Fig. 2b).

The tectono-stratigraphic sequence of the Precambrian rocks in the study area are arranged chronologically from the oldest to the youngest as follows; ultramafic rocks, ophiolitic metagabbros, biotite hornblende gneiss, monzogranite, syenogranite, garnetiferous muscovite granites as well as post granite dykes and veins.

The ultramafic rocks are found as sub-rounded masses varying in size from a few meters to mountain block size. It exhibits light brown color, soft and compact. **Ophiolitic metagabbros** form relatively low to medium relief topographic terrain and highly deformed with well exposed mesoscopic structure that are marked by the frequent presence of boudinage quartz veins extending parallel to the foliation planes (Fig. 3a). **The biotite hornblende gneiss rocks** form the huge masses of G. Hafafit, which represent the highest peaks in the studied area and occurs as fine to medium-grained, black to light grey in color and are characterized by sub-horizontal and vertical major joints (Fig. 3b). **Monzogranite** occurs at G. Nugrus (Fig. 3c) and G. Hafafit. It is characterized by massive, medium to coarse-grained size, buff to greyish buff in color showing boulder appearance, exfoliated and cavernous structures due to extensive deformation and weathering make it difficult for sampling (Fig. 3d). The rock is dissected by a master strike-slip fault striking nearly N-S and dipping 40°/SE. Minor normal faults are also recorded trending NW-SE and nearly dipping in E-W direction. **Syenogranite** form moderate to high relief mountain terrains at G. Magal El Harami (Fig. 3e), it is characterized by white to grey color, coarse-grained rocks and occasionally in the form of pegmatitic appearance. **The garnetiferous muscovite granite** is exposed at the northern part of G. Magal El Harami and occurs as medium to coarse-grained rocks, grey to whitish grey in color. It is characterized by highly foliated, jointed with brownish-red garnet grains that are commonly visible by naked eye (Fig. 3f).

The studied area is traversed by few post-granite dykes and veins (mostly basic dykes, quartz veins and veinlets).

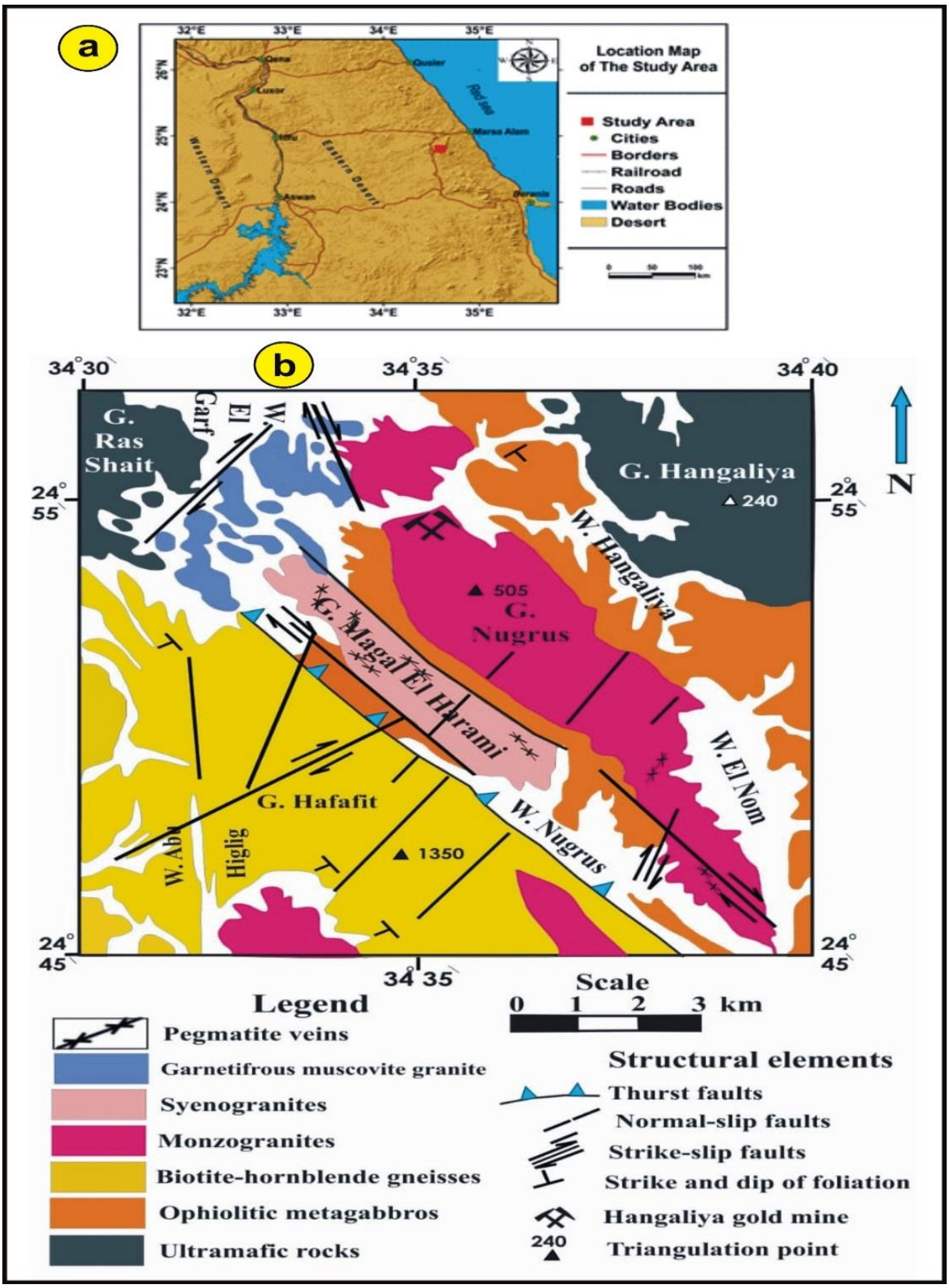

Fig. (2): (a) Location map (b) Geological map of G. Nugrus and G. Magal El Harami area, SED, Egypt modified after (mapping of G. M. Saleh 2011).

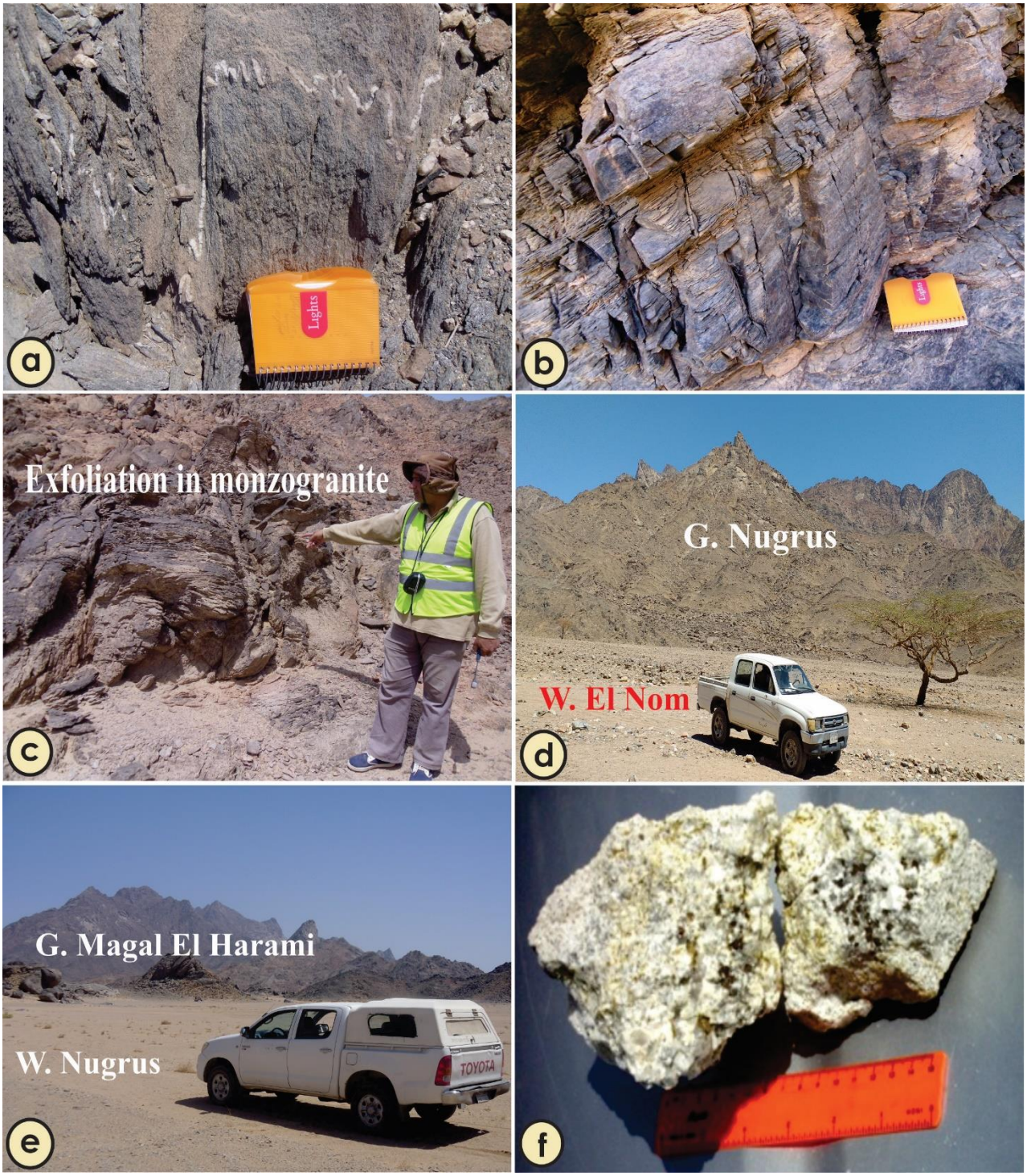

Fig. (3): Field photographs showing: **(a)** Well exposed mesoscopic structure in ophiolitic metagabbros at G. Magal El Harami, SED, Egypt. Looking N 45° E, **(b)** Subhorizontal and vertical major joints of biotite hornblende gneisses at G. Hafafit, SED, Egypt. Looking N 60° E, **(c)** Exfoliation in monzogranite rocks at G. Nugrus, SED, Egypt. Looking N 65° E and **(d)** Moderate to high rugged topography of G. Nugrus, SED, Egypt. Looking N 40° W, **(e)** Moderate to high relief mountain terrains of G. Magal El Harami, SED, Egypt. Looking N 45° E. **(f)** Slab of garnetiferous muscovite granites showing brownish-red garnet at G. Magal El Harami, SED, Egypt

3. METHODOLOGY

The study area was geologically mapped for the different rock lithologies and 15 samples (comprising 5 samples for monzogranite, 5 samples for syenogranite and 5 samples for garnetiferous muscovite granites) were collected for petrographic studies. Thin sections were prepared and investigated under polarizing microscope combined with a digital camera at the Laboratories of Nuclear Materials Authority (NMA), Cairo, Egypt to identify the mineral constituents and main textures. The selected samples of mineralized granites have been crushed to −60 mesh size followed by the quartering of crushed sample to obtain a representative sample of about 100 g for each one. The heavy minerals were separated using heavy liquid bromoform separation technique, followed by magnetic fractionation using a Frantz isodynamic separator. The heavy minerals were picked under a binocular microscope and identified by Scanning Electron Microscope (SEM) back-scattered images supported by energy-dispersive spectrometer (EDS) unit (model Philips XL 30 SEM) at the laboratory of the Nuclear Materials Authority (NMA) of Egypt. The field ground γ-ray spectrometry survey has been carried out using γ-ray spectrometric multi-channel analyzer instrument model RS-230 Canadian Type. Ground γ-ray spectrometric survey can detect dose rate (D.R.) in unit (nanosieverts per hour ($nSvh^{-1}$)), potassium (K%), equivalent uranium content (eUppm), and equivalent thorium content (eThppm). Uranium mobilization (eUm) in the studied rock types can be calculated from the difference between the measured eU and the expected original uranium, which is calculated by dividing the measured eTh by the average eTh/eU ratio in the crustal acidic rocks (original uranium = eTh/3.5, according to Clarke et al. [11] to give the leaching values of uranium (eUm = eU–eTh/3.5). Positive values indicate uranium addition by mobilization, whereas negative values indicate migration of uranium by leaching.

4. RESULTS AND DISCUSSIONS

4.1. Petrography of granitic rocks

Monzogranite is composed of plagioclase, potash feldspars, quartz and biotite as essential minerals, while zircon and opaques are observed as accessories.

Plagioclase is represented by albite and oligoclase, which occurs as twinned subhedral to euhedral crystals exhibiting a wide range of grain sizes, that is occasionally enclosing fine aggregates of quartz. Sometimes, it shows corrosion boundaries with quartz and slightly saussiritized (Fig. 4a). Potash feldspars are recognized by microcline and microcline microperthite that are observed in subordinate amounts as anhedral to subhedral crystal showing the characteristic cross-hatching pattern. Potash feldspars area commonly corroded and surrounded by subordinate amounts of plagioclase and quartz. Quartz is fine to medium-grained, subhedral to anhedral crystals with wavy extinction filling the interstitial grains between feldspar crystals. Biotite occurs as euhedral to subhedral elongate to flakey crystals and sometimes corroded by quartz and microperthite. It shows intensive alteration to chlorite, epidote, and opaque, which usually starts along the cleavage plane. Some crystals are considered as good hosts for most of the accessory minerals as zircon (Fig. 4b). Zircon occurs as well-formed crystals exhibiting its characteristic interference colors and occasionally included in biotite and sometimes surrounded by pleochroic halos. Opaques form irregular patches usually associated with biotite.

Syenogranite is composed essentially of potash feldspar, plagioclase, quartz, biotite, while zircon and titanite are the main accessory minerals. Chlorite and sericite are detected as secondary minerals. Potash feldspar occurs as euhedral to anhedral crystals and is represented by orthoclase microperthite and microcline microperthite. String perthite is dominated and fine crystals of plagioclase are poikilitically hosted within it. Sometimes, perthite corrodes and partially altered to sericite associated with plagioclase and quartz. Also, antiperthitic texture is observed. Plagioclase crystals are medium to coarse-grained, euhedral to subhedral elongated crystals. They have albite to oligoclase composition and exhibit albite and combined albite and pericline twinning. Plagioclase crystals show normal zoning and selective alteration. In some cases, plagioclase is affected by partial sericitization and

kaolintization (Fig. 4c). Quartz occurs as subhedral to anhedral coarse to medium crystals exhibit wavy extinction with few suture edges due to deformation. Quartz occupies the interstitial spaces between the other constituents or corrodes plagioclase, perthite and biotite. Phenocrysts of quartz are found surrounded by fine crystals of plagioclase. Biotite occurs as fresh brownish subhedral to euhedral flakes, up to filling the interspaces among the early crystallized plagioclase crystals. It also occurs as fine anhedral to subhedral crystals, usually kinked and strongly pleochroic from yellowish brown to dark brown color (Fig. 4d). Zircon occurs as a small crystal with very high relief, colorless and rimmed by iron oxides. It is present individually or as twinned crystals exhibiting parallel twinning. Sometimes, it is enclosed within other minerals such as biotite and plagioclase. Zircon grains are commonly fractured metamicted and surrounded by pleochroic haloes due to radiation damage from the radioactive inclusions (Fig. 4e). Titanite is present as well-formed crystals with sphenoidal form associating the main constituents and the other accessory minerals.

Garnetiferous muscovite granites are composed of quartz, potash feldspar plagioclase, muscovite and garnet while, zircon, kyanite, cordierite and opaques are the main accessory minerals. Sericite, chlorite and kaolinite are secondary minerals.

Quartz occurs as subhedral to anhedral crystal, fine to medium- grains, showing undulose extinction. The larger quartz crystals are fractured with serrate sub-grain boundaries and the finer crystals are squeezed to form thin bands due to intensive stress. Potash feldspar occurs as subhedral crystal and commonly corroded by quartz and perthites.

Plagioclase is euhedral to subhedral crystals, exhibits lamellar twinning and normal zoning due to variation in composition from Ca-rich core to Ca-poor rim. Garnet is the main accessory mineral occurring as well-formed polygonal crystals of magmatic origin, some garnet crystals enclose a nucleus of another mineral surrounded by radial fractures and may be radioactive (Fig. 4f). Muscovite is represented by small to medium flakes exhibiting characteristic high interference colors, filling the fracture of quartz (Fig. 4g). Zircon occurs as small prismatic crystals associated with the other constituents (plagioclase, quartz and microcline). Allanite occurs as minute crystals with high relief, reddish-brown to dark honey yellow in color and sometimes zoned at their rims (Fig. 4h). Cordierite forms subhedral to anhedral crystals as porphyroblasts embedded within fine quartz and potash feldspars. Kyanite occurs as subhedral to euhedral crystals that are characterized by colorless to pale blue, high relief, perfect cleavage. Opaques are found in the form of scattered small subhedral grains and anhedral interstitial skeletal crystals.

4.2. Mineralogical investigations

The different granitic rocks have been examined for their radioactive, opaque and other essential minerals. The identified minerals are uranophane, uranothorite, monazite, xenotime, allanite, fergusonite, zircon, pyrite, sphalerite, arsenopyrite, chalcocite, chalcopyrite, gold and krennerite

4.2.1. Uranophane [$Ca(UO_3)_2(SiO_2)_2(OH)_2,5H_2O$] is hydrated calcium uranium silicate. It is resulted from the alteration process of uraninite and the chief constituent of the outer silica zone of uraninite alteration. It is dimorphs with beta-uranophane [12]. The uranophane is confirmed by SEM techniques that contains 65.72% U, 13.96% Si, 5.65% Al and 1.76% Fe (Fig. 5a).

4.2.2. Uranothorite (U,Th) SiO_4 is crystallized in the tetragonal system, isomorphous with zircon and strongly radioactive mineral. It is worthy to mention that zircon ($ZrSiO_4$) and thorite (ThO_4) form a structural series by adding U and Th and loss of silica [13]. The uranothorite is confirmed by SEM techniques and contains 68.10% Th, 14.35% U, 9.46% Si, and 4.11% Fe (Fig. 5b).

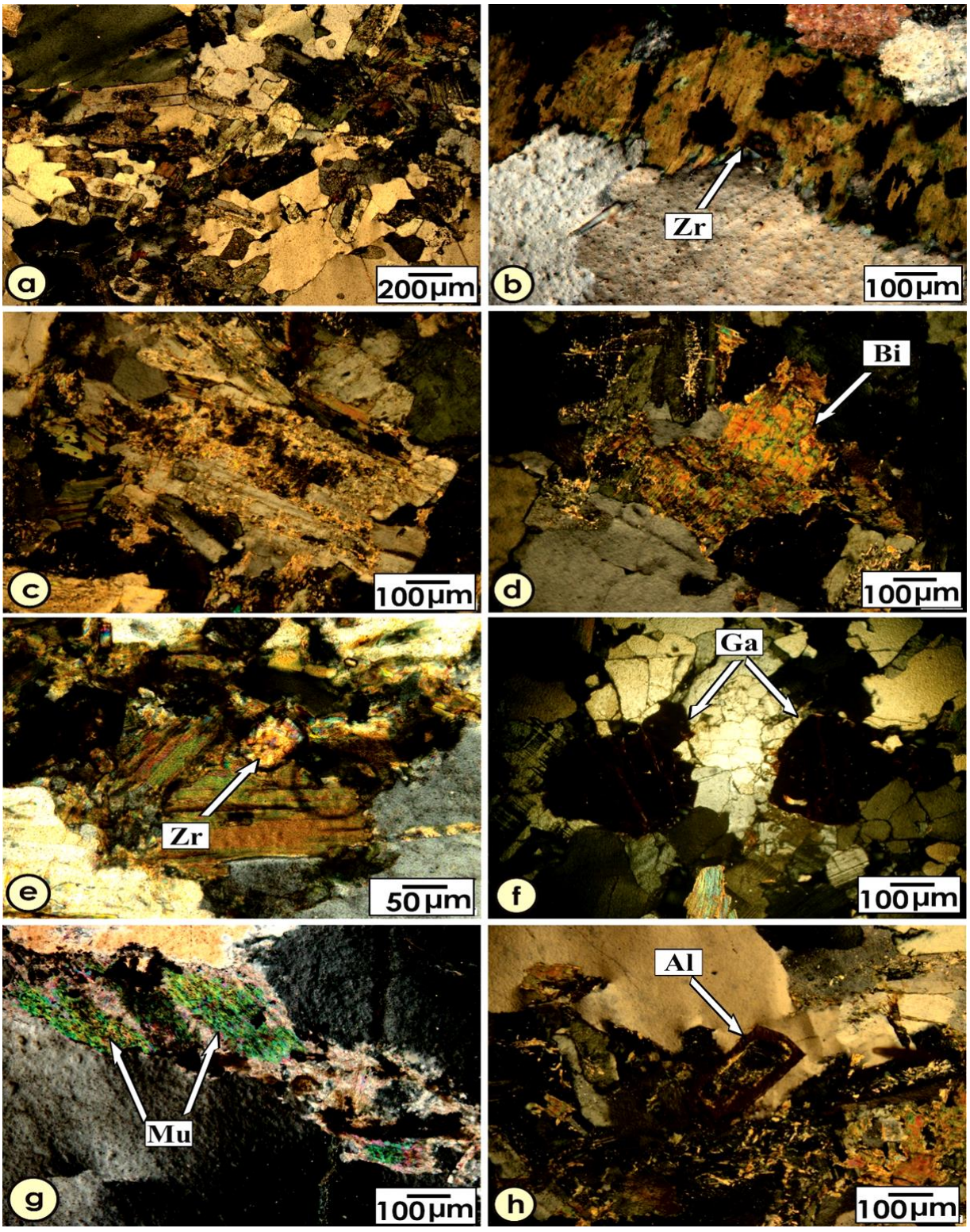

Fig. (4): Photomicrograph showing: **(a)** Crowded fine crystals of plagioclase and biotite in monzogranite (C.N), **(b)** Flakes of biotite enclosing euhedral crystal of zircon (Zr) in monzogranite (C.N), **(c)**Plagioclase partially altered to sericite in syenogranites (C.N), **(d)** Kinked biotite (Bi) crystal associated with quartz, perthite and plagioclase(C.N), **(e)** Zircon (Zr) partially martitized associated with biotite in syenogranite (C.N). **(f)** Polygonal crystals (Ga) of garnet associating the main constituents of the rock in garnetiferous muscovite granites (C.N), **(g)** Secondary muscovite (Mu) filling the fracture in quartz in garnetiferous muscovite granites (C.N) and **(h)** Zoned allanite (Al) crystal in garnetiferous muscovite granites (C.N)

4.2.3. Monazite [(Ce,La,Nd,Th)PO_4] is considered to be radioactive mineral, so it is a useful mineral for radiometric dating of different geological events, such as crystallization, heating or deformation of the rocks. It is detected by SEM and contains 29.75% Ce, 18.68% La, 4.11% Th, 10.22% Nd, 3.84% Pr, 1.07% U, 10.77% P, 1.71% Gd, and 2.29% Sm (Fig. 5c).

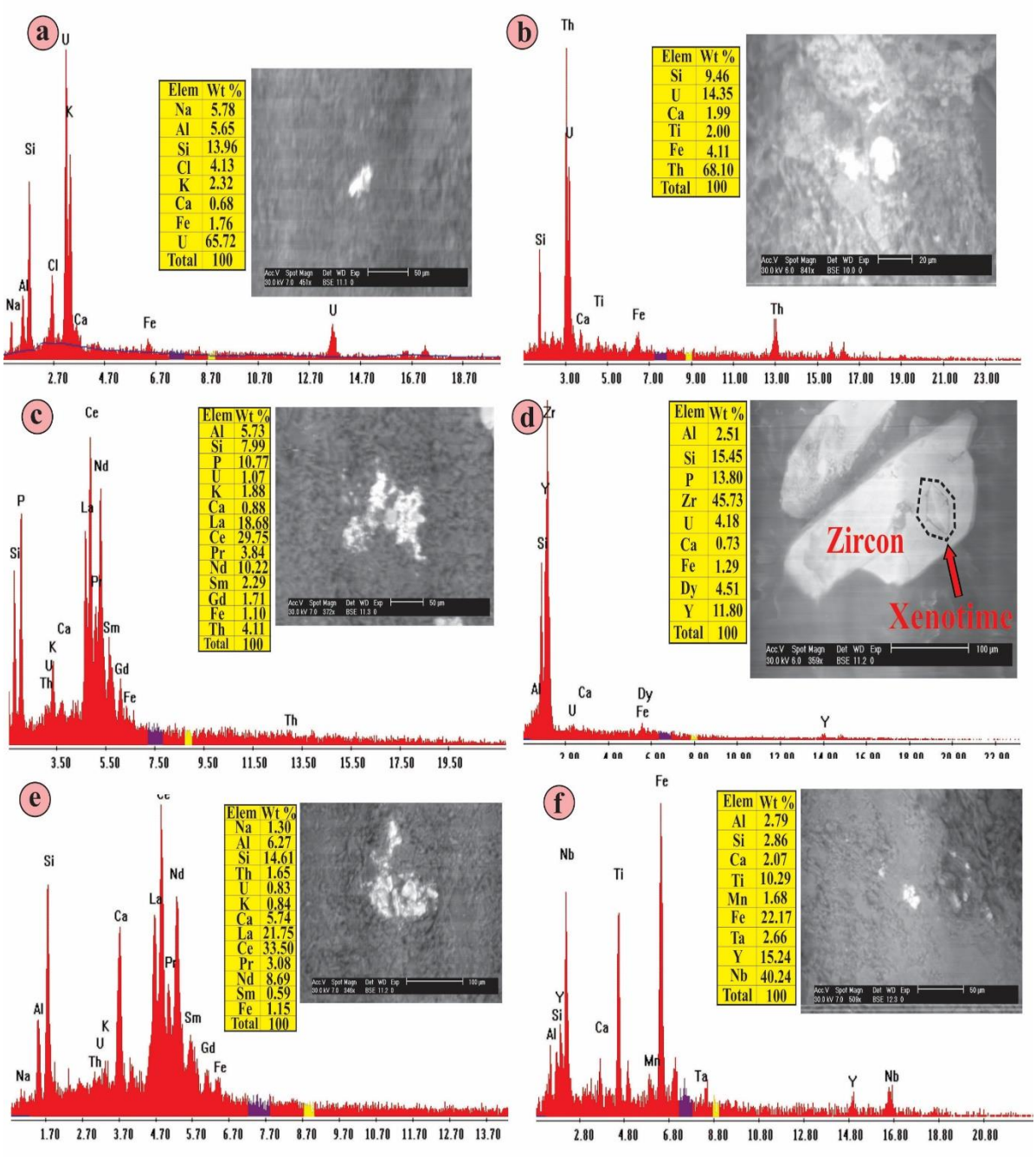

Fig. (5): (a) SEM spectrograph and BSE image of **(a)** Uranophane, **(b)** Uranothorite, **(c)** Monazite, **(d)** Xenotime, **(e)** Allanite and **(f)** Fergusonite at garnetiferous muscovite granite rocks in G. Magal El Harami, SED, Egypt

4.2.4. Xenotime (YPO_4) is used chiefly as a source for Y and HREEs (Dy, Yb, Er and Gd). The SEM techniques detected the presence of xenotime enclosed within zirconium crystal. It contains 45.73% Zr**,** 13.80% P, 2.51% Al**,** 15.45% Si**,** 11.80% Y**,** 4.18% U and 4.51% Dy (Fig. 5d).

4.2.5. Allanite $(Ca,Ce)_2(Al,Fe_2+,Fe_3+)_3(SiO_4)(OH)$ contains some thorium, up to 3 percent Berry et al., 2000 [14]. The non-metamict allanite is distinguished from other epidotes by their brownish color and from the metamict ones by their isotropic character under polarizing microscope Deer et al., 1992 [15]. It is confirmed by SEM techniques and contains 5.74% Ca, 21.75% La, 33.50% Ce, 8.69% Nd, 1.65% Th, 0.83% U, 3.08% Pr, 0.59% Sm and 1.15% Fe (Fig. 5e).

4.2.6. Fergusonite [(Y,Er) $(Nb,Ta,Ti)O_4$] may contain significant quantities of U and Th, and thus it is commonly metamict [16-18]. It is measured by SEM that contains 40.24% Nb, 22.17% Fe, 15.24% Y, 2.66% Ta, 10.29% Ti, 2.79% Al, 2.86% Si, and 2.07% Ca (Fig. 5f).

4.2.7. Zircon [$Zr(SiO_4)$] is a common accessory mineral in a wide range of rocks, particularly in felsic igneous rocks [19;20]. The importance of this accessory mineral lies in a combination of factors, including its tendency to incorporate trace elements (including radionuclides), [21; 22]. Although the abundance of zircon is low, it strongly affects the behavior of many trace elements during the crystallization of magmas, and understanding of its chemistry therefore is an important step for petrological modeling [23-25]. The studied zircon is characterized by prismatic and bi-pyramidal crystals and has varying shades of honey color (Fig. 6a). It is confirmed by SEM techniques with 54.14% Zr, 33.85% Si, 6.34% Hf, 2.20% Fe and 3.47% Ca (Fig. 6b).

4.2.8. Pyrite [FeS_2] occurs as isometric crystals that usually appear as cubes. Pyrite has pale-brassy to golden-yellow color with metallic luster and black streak (Fig. 6c). Pyrite is detected by SEM techniques that contain 47.86% S, and 47.50% Fe, 2.17% Al and 2.46% Si (Fig. 6d).

4.2.9. Sphalerite (ZnS) is the major source not only of Zn, but also of Cd, In, Ge, and Ga [26]. It is confirmed by SEM techniques that it contains 47.61% Zn and 25% S, 17.04% Si, 2.14% Al, 6.89% Fe and 1.33% K (Fig. 7a).

4.2.10. Arsenopyrite (FeAsS) is found in pegmatites, high-temperature gold-quartz, veins and in contact metamorphic sulfide deposits; less commonly of low-temperature hydrothermal origin. Arsenopyrite is confirmed by SEM techniques, it contains 44.58% As, 32.49% Fe, 18.69% S and 2.89% Si (Fig. 7b).

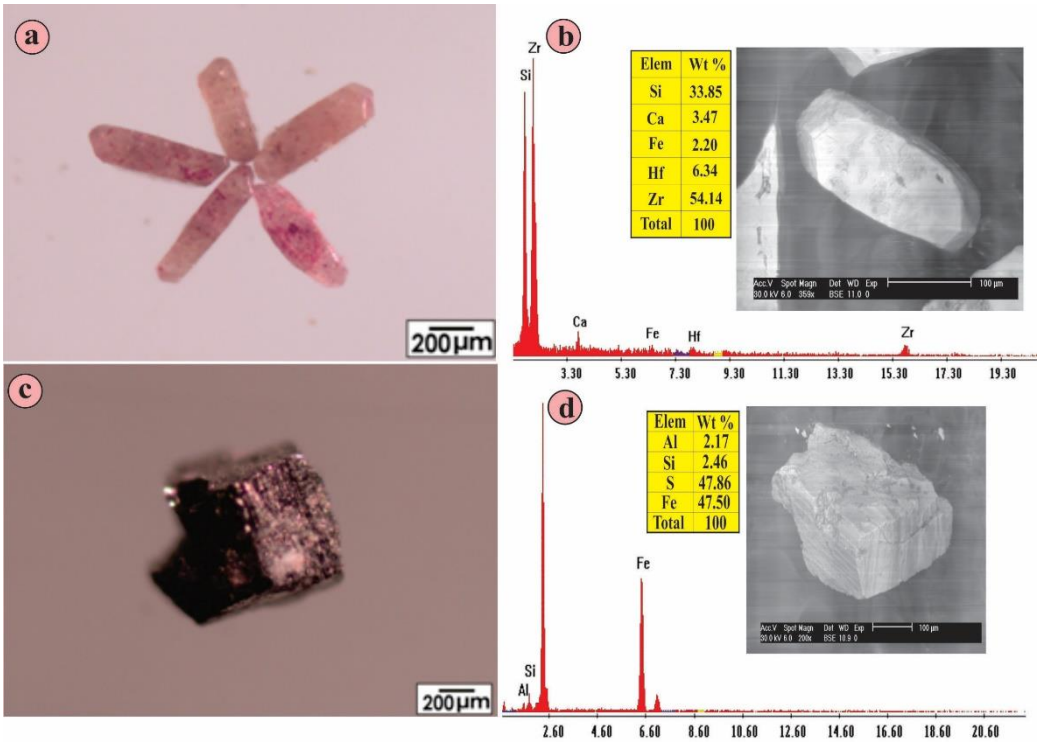

Fig. (6): (a) Photomicrograph showing zircon grains with honey color, **(b)** SEM spectrograph and BSE image of prismatic zircon at garnetiferous muscovite granite rocks in G. Magal El Harami, SED, Egypt. **(c)** Photomicrograph showing pyrite grains with cubic form, **(d)** SEM spectrograph and BSE image of pyrite at monzogranite rock of G. Nugrus in Hangaliya gold mine, SED, Egypt

4.2.11. Chalcocite (Cu_2S) occurs in the supergene environment below the oxidation zone of copper deposits as a result of its leaching from the oxidized minerals. The EDX analysis of chalcocite mineral indicates that it contains 73.31% Cu, 24.22% S and 2.47% Si (Fig. 7c).

4.2.12. Chalcopyrite ($CuFeS_2$) is a very common copper mineral that occurs as an exsolution product in mafic igneous rocks, tetragonal, equant and tetrahedral-shaped crystals. It is confirmed by SEM techniques and contains 23.07% Cu, 29.85% Fe, 29.87% S, 1.99% Al, 10.05% Si and 2.38% As (Fig. 7d).

4.2.13. Gold (Au) is usually associated with pyrite and other sulfide minerals. In the study area, gold is found in the native form. The EDX data shows 69.43% Au, 25.99% Ag, 1.49% Cu and 2.49% Si (Fig. 7e).

4.2.14. Krennerite (Au_3AgTe_8) the general formula is $AuTe_2$, but specimen with gold substituted by up to 41.32% with silver have been found. Both of the chemically similar gold-silver telluridescalaverite and sylvanite are in the monoclinic crystal system, whereas kennerite is orthorhombic. The EDX data shows 20.39% Au, 41.32% Ag, 32.82% Te, 2.88% Si and 2.59% Fe (Fig. 7f).

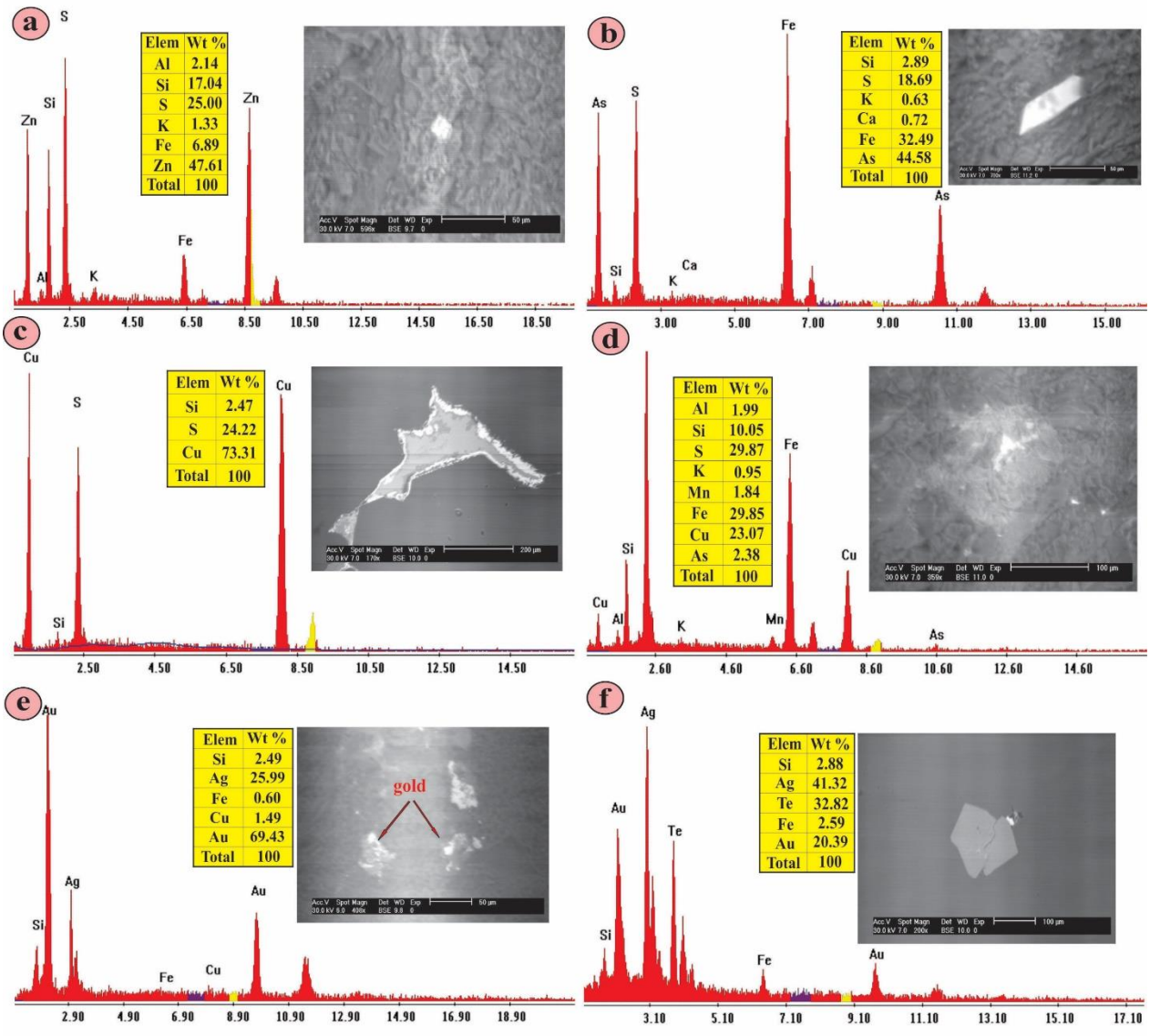

Fig (7): SEM spectrograph and BSE image of **(a)** Sphalerite, **(b)** Arsenopyrite, **(c)** Chalcocite, **(d)** Chalcopyrite, **(e)** Gold and **(f)** Krennerite at monzogranites rock of G. Nugrus in Hangaliya gold mine, SED, Egypt

4.3. Spectrometric prospecting

The ranges and average of eU, eTh and K% for the studied monzogranites at north and south of G. Nugrus, syenogranite and garnetiferous muscovite granites at G. Magal El Harami are listed in Table (1). The average eU, eTh and K% contents in both north and south monzogranite of G. Nugrus are 9.25ppm, 5.4ppm, 31.41ppm, 19.29ppm, 6.08% and 3.96% respectively. The average of eU in north G. Nugrus is more than twice Clark value (4ppm for normal granites), and, therefore, they can be considered as uraniferous granites.

The binary relations of eU, eTh, eU/eTh and eU-eTh/3.5 may provide an indicator of the geochemical behavior of U and Th in the studied rock samples. In the monzogranite of north G. Nugrus (Fig. 8a to f), most of the radiometric measurements plot around the ratio of eU/eTh = 0.5, which means magmatic origin and some enrichment with uranium. There are strong positive relations between K% versus eU (r = 0.87), K% versus eTh (r = 0.89) and eU versus eU/eTh (r= 0.71). There is a negative relation between eTh versus eU/eTh (r = -0.07). The relation of eU versus eU-eTh/3.5, indicates addition of uranium in some samples and depletion from the others.

In the monzogranite of south G. Nugrus (Fig. 9a to f), there is a negative relation between eTh versus eU/eTh ratio (r= -0.07) and there are strong positive relations between eU versus eU/eTh (r = 0.71), K% versus eU (r = 0.69), K% versus eTh (r = 0. 89).The relations between eU with (eU-eTh/3.5) and most of the radiometric measurements plot between the ratio of eU/eTh = 0.5 and 0.125 indicates slight addition of uranium.

In the syenogranite, the average eU, eTh and K% contents are 10.22ppm, 24.45ppm and 2.96% respectively. The average of eU is more than twice the Clark value (4ppm for normal granites), and, therefore, they can be considered as uraniferous granites. Most of the radiometric measurement plots are around the ratio of eU/eTh = 0.5. There is a negative relation between eTh versus eU/eTh ratio (r= -0.33), while there is a weak positive relation between eU versus eU/eTh ratio (r= 0.015). There are moderate positive relations between K% versus eU (r = 0.18) and K% versus eTh (r = 0.42). The relation between eU with (eU-eTh/3.5) indicates the addition of uranium for some samples (Fig. 10a to f).

In the garnetiferous muscovite granite, the average eU, eTh and K% contents are 7.82 ppm, 13.33ppm and 3.32% respectively. Most of the radiometric measurements plot between the ratio of eU/eTh = 1.0-0.125. There are negative relations between eTh versus eU/eTh ratio (r= -0.25) and K% versus eU(r= -0.04). There is a strong positive relation between eU versus eU/eTh (r = 0.85) and weakly positive relation of K% versus eTh (r = 0.08). The relations between eU and (eU-eTh/3.5) indicate some addition of uranium (Fig. 11a to f). The highest concentration of uranium exists in syenogranite, south of G. Magal El Harami, while the highest thorium concentration occurs in monzogranite of north G. Nugrus (Fig. 12).

Table (1): Spectrometric measurements of the range and average contents of K (%), eU (ppm), eTh (ppm), eU/eTh and eUm in the different rock units at and around G. Nugrus area, SED, Egypt

The area	K%		eU (ppm)		eTh (ppm)		eU/eTh		eUm	
	Ranges	Av.	Ranges	Av.	Ranges	Av.	Ranges	Av.	Ranges	Av.
Monzogranite at north G. Nugrus (N=28)	**3.9-9.6**	**6.08**	**4.5-16.7**	**9.25**	**21.6-45.9**	**31.41**	**0.16-0.49**	**0.3**	**-5.41-4.87**	**0.28**
Monzogranite south G. Nugrus (N=28)	**1.0 -5.7**	**3.96**	**2.2-8.1**	**5.4**	**4.6-28.8**	**19.29**	**0.15-1.39**	**0.34**	**-3.34-5.09**	**0.13**
Syenogranite in south G. Magal El Harami (N=86)	**0.9-5.3**	**2.96**	**2.2-29.6**	**10.22**	**1.4-69.2**	**24.45**	**0.14-2.71**	**0.50**	**-5.04-17.43**	**3.23**
Garnetiferous muscovite granite at north G. Magal El Harami (N=21)	**1.8-4.7**	**3.32**	**2.2-22**	**7.82**	**6-27**	**13.33**	**0.22-2**	**0.63**	**-1.14-18.86**	**4.01**

N= number of radioactive measurements, Av.= Average

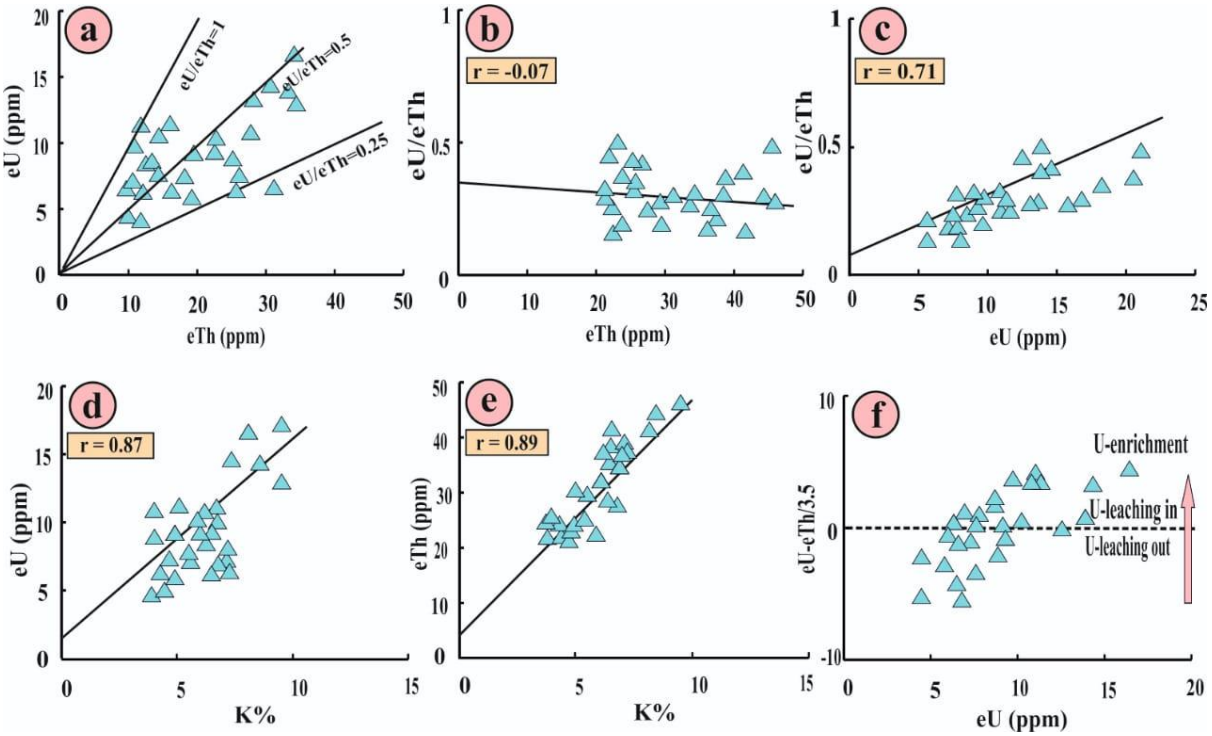

Fig. (8): The relation between a) eU versus eTh, b) eU/eTh versus eTh, c) eU/eTh versus eU, d) eU versus K%, e) eTh versus K% and f) (eU-eTh/3.5) versus eU, within monzogranite at north G. Nugrus, SED, Egypt

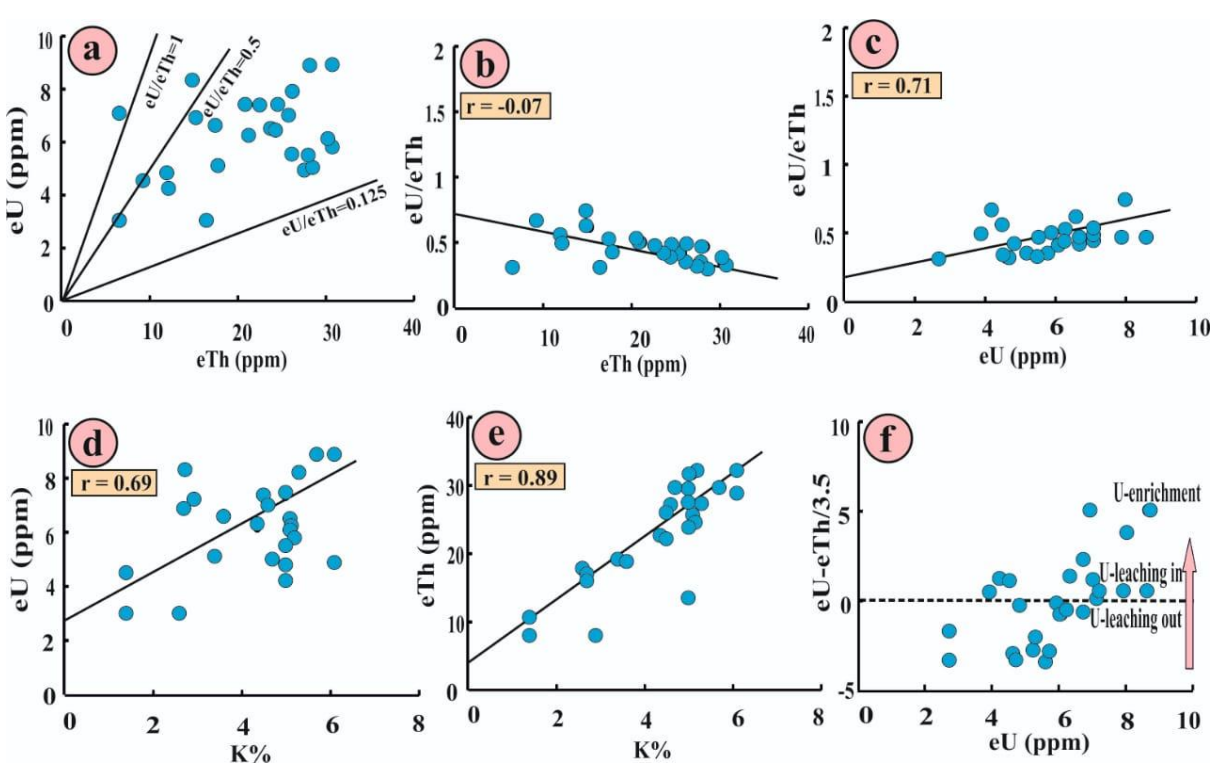

Fig. (9): The relation between a) eU versus eTh, b) eU/eTh versus eTh, c) eU/eTh versus eU, d) eU versus K%, e) eTh versus K% and f) (eU-eTh/3.5) versus eU, within the monzogranite in south of G. Nugrus area, SED, Egypt

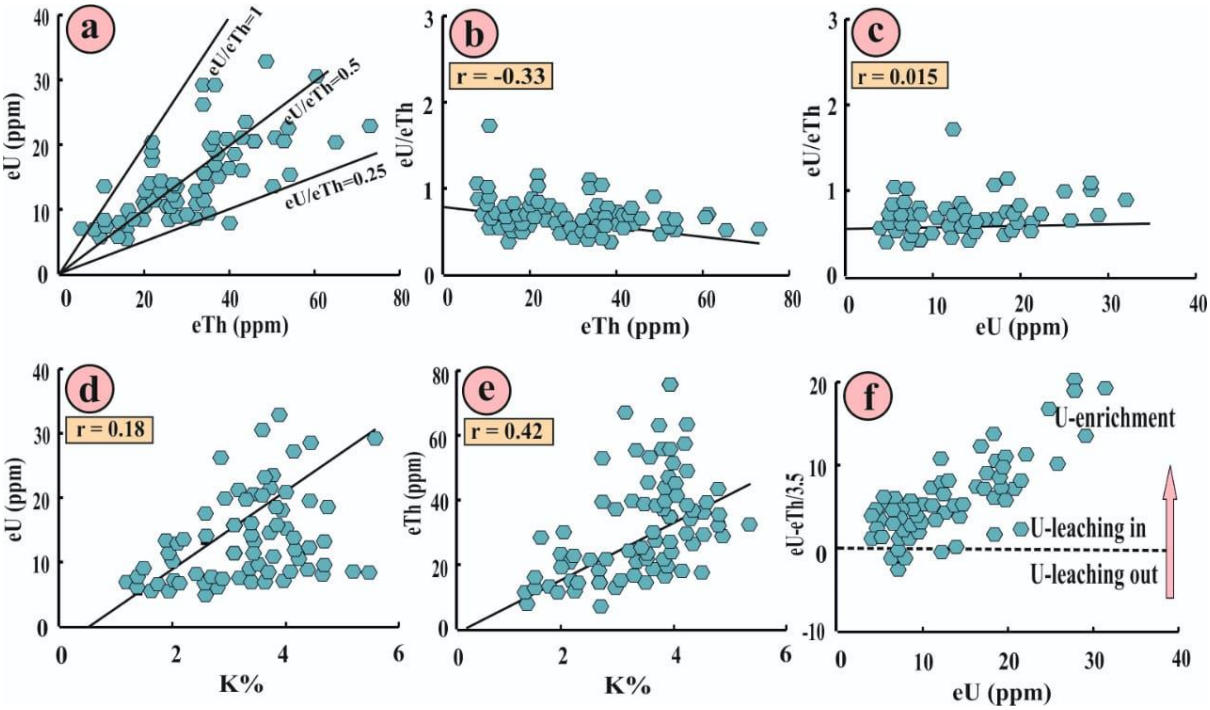

Fig. (10): The relation between a) eU versus eTh, b) eU/eTh versus eTh, c) eU/eU versus eU, d) eU versus K%, e) eTh versus K% and f) (eU-eTh/3.5) versus eU, within syenogranite in south G. Magal El Harami area, SED, Egypt

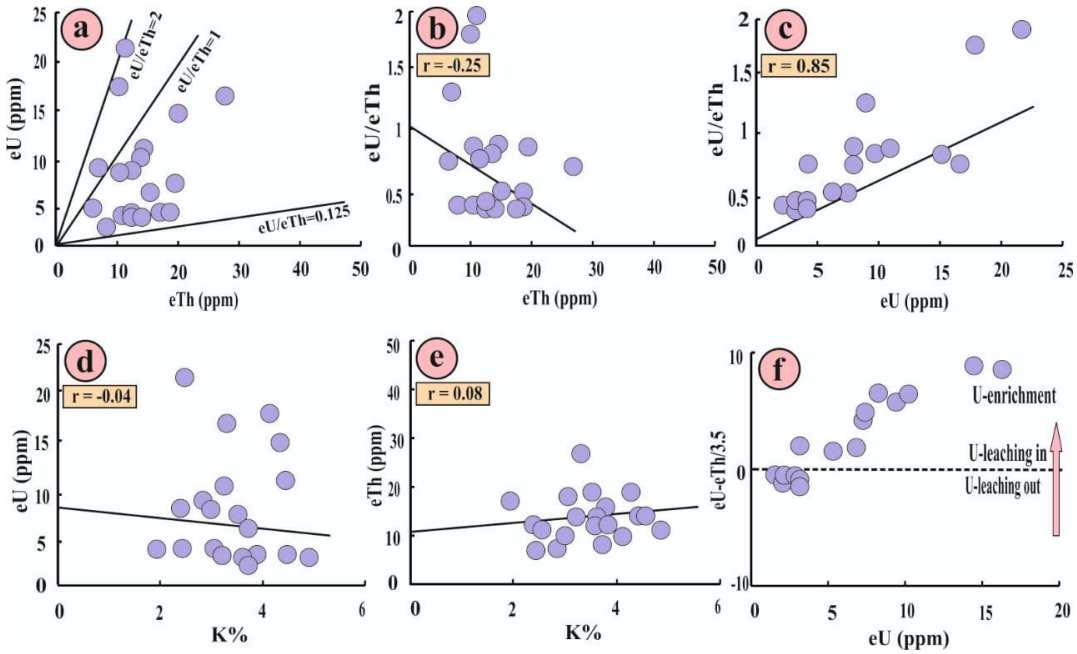

Fig. (11): The relation between a) eU versus eTh, b) eU/eTh versus eTh, c) eU/ eTh versus eU, d) eU versus K%, e) eTh versus K% and f) (eU-eTh/3.5) versus eU, within garnetiferous muscovite granite in north G. Magal El Harami area, SED, Egypt

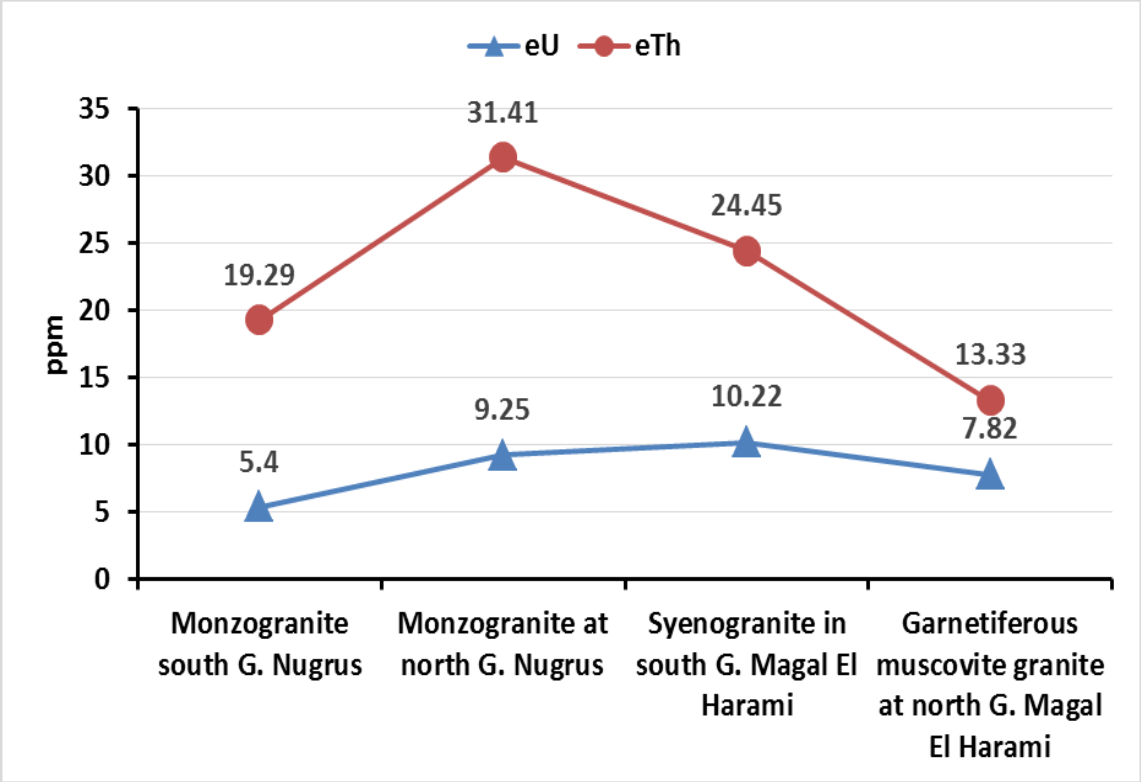

Fig. (12): Profile line diagram showing the average concentration of uranium and thorium in the different granitic rocks at and around G. Nugrus area, SED, Egypt

4.3. Radioactive anomaly

The radioactive anomaly in the study area is confined to the fractures cutting the garnetiferous muscovite granite at the northern part of G. Magal El Harami area (2.5m X 3m in dimension). The minimum, maximum and average of K%, eU, eTh and eUm values are illustrated in Table (2). The potassium percent for the studied rock units ranges from 1.6 to 5.9 with an average of 3.76%. The eU contents ranges from 25 to 445ppm with an average of 187.87ppm, the eTh content ranges from 10 to 321ppm with an average of 109.57ppm, the eU/eTh ratios ranges from 0.41 to 3.62 with an average of 1.99, the eUm ranges from 8.94 to 380.71 with an average of 156.57 reflecting strong addition of uranium.

The binary relations of K%, eU, eTh, and eTh/eU are illustrated in Fig. (13a to f). The variation diagrams of the studied granites at north G. Magal El Harami show that; most of the radiometric measurements are plotted between the ratio eU/eTh= 3.0 -1.0. There are moderate positive relation between K% versus eTh (r = 0.36) and eU (r= 0.29), while there are negative relation between the ratio eU/eTh with both eTh (r= -0.54) and eU (r= -0.30). The relation between eU versus eUm, shows strongly positive relation, indicating a strong addition of uranium from the surrounding rocks.

Table (2): The minimum, maximum and the average of K (%), eU (ppm), eTh (ppm), eU/eTh and eUm in the radioactive anomaly of garnetiferous muscovite granite at the northern part of G. Magal El Harami, SED, Egypt

N=44	K%	eU (ppm)	eTh (ppm)	eU/eTh	eUm
Min	1.6	25	10	0.41	8.94
Max	5.9	445	321	3.62	380.71
Average	3.76	187.87	109.57	1.99	156.57

N=number of radioactive measurements, Min= minimum, Max= maximum

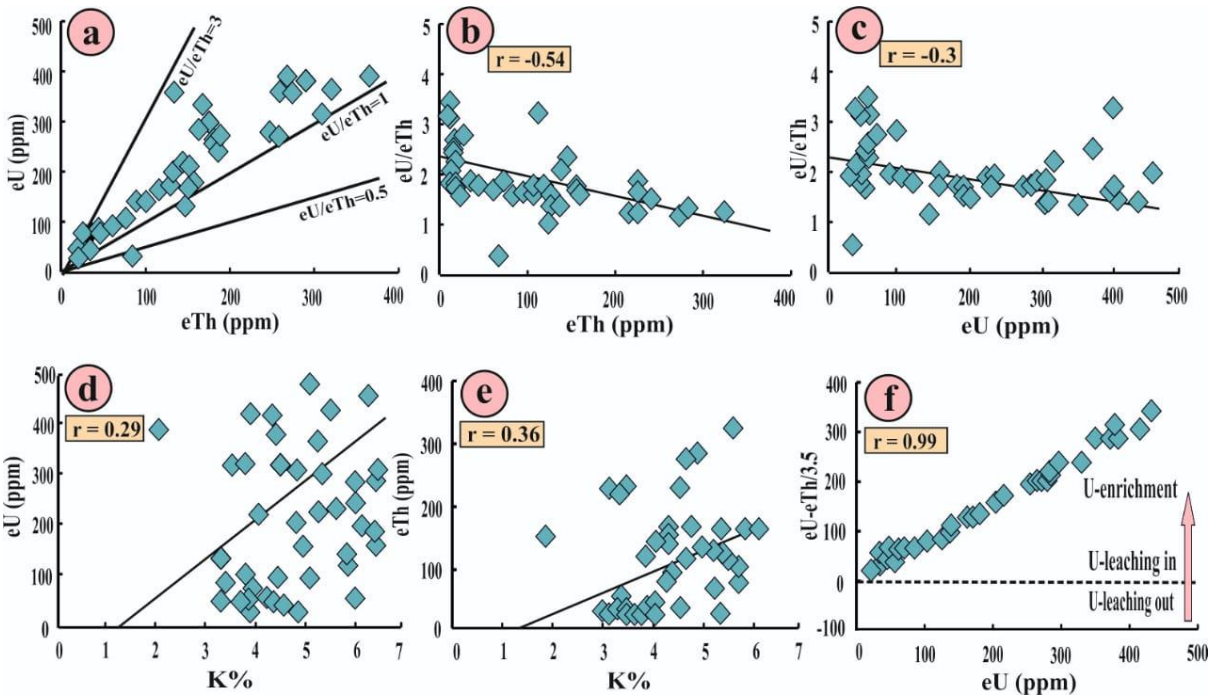

Fig. (13): The relation between a) a) eU versus eTh, b) eU/eTh versus eTh, c) eU/eU versus eU, d) eU versus K%, e) eTh versus K% and f) (eU-eTh/3.5) versus eU, within the garnetiferous muscovite granites at north G. Magal El Harami area, SED, Egypt

4.4. Origin of uranium mineralization

Ore-genesis theories generally involve three components: source, transport or conduit, and trap. Source is required because the metal must come from somewhere, and be liberated by some process. Transport is required first to move the metal-bearing fluids or solid minerals into their current position, and refers to the act of physically moving the metal, as well as to chemical or physical phenomena, which encourage movement. Trapping is required to concentrate the metal via some physical, chemical, or geological mechanism into a concentration, which forms a mineable ore. The biggest deposits form when the source is large, the transport mechanism is efficient, and the trap is active and ready at the right time.

The evidences of the presence of the radioactive anomalies in the area under study can be assumed on the bases of:

1- The presence of radioactive anomalies along fractures.

2- The existence of some accessory minerals that can carry U and Th.

3- Records of intensive alteration of some primary minerals.

From the previously mentioned notes, it can be concluded that, the magmatic role has its print and the post-magmatic changes is clear and cannot be neglected in the formation of radioactive anomalies as follows: in the studied area, uranium dissolved from the surrounding area (different types of granites) by meteoric /ground water through joints and fractures and finally deposited/ trapped along the fractures of garnetiferous muscovite granites (absorbed by iron oxides) and less impermeable mica lenses due to change in the physicochemical conditions, Eh and Ph.

5. CONCLUSIONS

The area under study is covered by ultramafic rocks, ophiolitic metagabbros, biotite hornblende gneiss, monzogranite, syenogranite and garnetiferous muscovite granites. The investigated area has apparently been subjected to extensional forces that led to the intrusion of a large number of dykes and quartz veins. Petrographically, monzogranite is composed of plagioclase, potash feldspars, quartz and biotite as

essential minerals, while zircon and opaques are accessory minerals. Syenogranite is composed essentially of potash feldspar, plagioclase, quartz, biotite, while zircon and titanite are accessories. Chlorite and sericite are secondary minerals. Garnetiferous muscovite granite is composed essentially of quartz, potash feldspar plagioclase, muscovite and garnet while zircon, kyanite, cordierite and opaques are accessory minerals. Sericite, chlorite and kaolinite are secondary minerals.

The mineralizations in the studied area are uranophane, uranothorite, zircon, monazite, xenotime, allanite, sphalerite, arsenopyrite and pyrite. The spectrometric prospecting was carried out on the different younger granite rocks. In monzogranite, the average eU, eTh and K% contents in both north and south of G. Nugrus are 9.25ppm, 5.4ppm, 31.41ppm, 19.29 ppm, 6.08% and 3.96% respectively. In the syenogranite, the average eU, eTh and K% contents are 10.22ppm, 24.45ppm and 2.96% respectively. The average of eU in north G. Nugrus monzogranite and in syenogranite is more than twice Clark value (4 ppm for normal granites), therefore, they can be considered as uraniferous granites. In the garnetiferous muscovite granite, the average eU, eTh and K% contents are 7.82ppm, 13.33ppm and 3.32% respectively. The highest concentration of uranium exists in syenogranite, south of G. Magal El Harami, while the highest thorium concentration occurs in monzogranite of north G. Nugrus). The radioactive anomaly in the study area is confined to the fractures cutting the garnetiferous muscovite granite at the northern part of G. Magal El Harami area (2.5m X 3m in dimension). The eU content ranges from 25 to 445ppm with an average of 187.87ppm, the eTh content ranges from 10 to 321ppm with an average of 109.57ppm, the eU/eTh ratios ranges from 0.41 to 3.62 with an average of 1.99, the eUm ranges from 8.94 to 380.71 with an average of 156.57 reflecting strong addition of uranium from the surrounding rocks.

In the study area, the magmatic role has its print and the post-magmatic changes is clear and cannot be neglected in the formation of radioactive anomalies as follows: uranium dissolved from the surrounding area (different types of granites) by meteoric /groundwater through joints and fractures and finally deposited/ trapped along the fractures of garnetiferous muscovite granites (absorbed by iron oxides) and less impermeable mica lenses due to change in the physicochemical conditions, Eh and Ph.

REFERENCES

[1] Stern, R. J. and Hedge, C. E. (1985): Geochronology and isotope constrains on Late Precambrian crustal evolution in the Eastern Desert of Egypt. Am. J. Sci., 285, P. 97-127.

[2] El Gaby, S., List, F. K. and Tehrani, R. (1988): Geology, evolution and metallogenesis of the Pan African belt in Egypt. In: El-Gaby, S. & Greiling, R. O. (eds.): The Pan African belt of north east Africa and adjacent areas. Braun Schweig (Vieweg): P. 17-68.

[3] Hassan, M. A. (1998): Geology and geochemistry of Gabel Nugrus gneissose granite, central Eastern Desert, Egypt. Bull. Fac. Sci., Assiut Univ., 27 (2-f), P. 1-19.

[4] Salman, A. B., El-Assy, I. E. and Shalaby, M. H. (1990): New occurrences of uranium mineralization in Gebel Gattar, north Eastern Desert, Egypt. Annals Geol. Surv. Egypt, 16, P. 31–34.

[5] Shalaby, M. H. (1996): Structural controls of uranium mineralization at Gebel Gattar, north Eastern Desert, Egypt. Acad. Sci. Bull. Egypt, 46, 521–536.

[6] Bakhit, F. S. (1978): Geology and radioactive mineralization of Gebel El-Missikat area, Eastern Desert, Egypt. Ph.D. Thesis, Ain Shams Univ., Egypt, 289 p.

[7] El-Bayoumi, R. M., Hassan, M. A., Salman, A. B. and Abdallah, S. M. (1999): Subsurface geologic studies on Gebel El-Missikat uranium occurrence, central Eastern Desert, Egypt. Proc. 4th Intern. Conf. Geol. Arab World, Cairo Univ., Egypt, Feb. 1998, P. 541–564.

[8] El-Tahir, M. A. (1985): Radioactivity and mineralization of the granitic rocks of El-Erediya occurrence, Eastern Desert, Egypt. Ph.D. Thesis, Al-Azhar Univ., Egypt, 132 p.

[9] Mohamed, N. A. (1995): Distribution and extraction of uranium and some trace elements from the mineralized zones of El-Missikat El-Erediya area, Eastern Desert, Egypt. Ph.D. Thesis, Cairo Univ., Egypt, 185 p.

[10] Assaf, H. S., Ibrahim, M. E., Ammar, S. E., Saleh, G. M. and Rasheid, M. A. (1998): Geological and mineralogical studies on the radioactive mineral occurrence at Qash Amir area, Southeastern Desert,

Egypt. Internal Rep. Nuclear Materials Authority of Egypt. 41 p.

[11] Clarke, S. P. Jr., Peterman, Z. E., and Heier, K. S. (1966): Abundances in uranium, thorium and potassium. In Handbook of physical constants, Geological society of America, Memoir 97: P. 521–541.

[12] Gorman, D. H. and Naffield, E. W. (1955): Studies of radioactive compound: Uranophane and Beta-uranophane, An, Min, V. 40, P. 634–645.

[13] Heinrich, E. W. (1962): Mineralogy and geology of radioactive raw materials. Mc Graw-Hill Book Company, New York, 232 p.

[14] Berry, L. G., Mason, B. and Dietrich, R. V. (2000): Mineralogy. CBS publishers and distributors, New Delhi, India. 561 p.

[15] Deer, W. A., Howie, R. A. and Zussman. J. (1992): An introduction to the rock forming minerals. Longman group limited, England. Second edition. 696 p.

[16] Ervanne, H. (2004): Uranium oxidation states in allanite, fergusonite and monazite of pegmatites from Finland. Mineralogie, 7, P. 289–301.

[17] TomaŠić, N., Gajovi, C. A., Bermanec, V., Su, D. S., RajićLinarić, M., Ntaflos, T. and Schlögl, R. (2006): Recrystallization mechanism of fergusonite from metamict mineral precursors. Phy. Chem. Min., 33, P. 145–159.

[18] Reto, G., Terry, W., Richard, W. and Katja, R. (2009): Metamict fergusonite-(Y) in a spessartine-bearing granitic pegmatite from Adamello, Italy. Chem. Geol., 261, P. 333–345.

[19] Heaman, L. M., Bowins, R. and Crocket, J. (1990): The chemical composition of igneous zircon suites: implications for geochemical tracer studies. Geochimica et Cosmochimica Acta 54, P. 1597–1607.

[20] Hoskin, P. W. O. and Schaltegger, U. (2003): The composition of zircon and igneous and metamorphic petrogenesis. In: Hanchar, J. M. and Hoskin, P.W.O. (eds) Zircon. Reviews in Mineralogy and Geochemistry 53, P. 27–62.

[21] Watson, E. B. (1996): Dissolution, growth and survival of zircons during crustal fusion: kinetic principles, geological models and implications for isotopic inheritance. Transactions of the Royal Society of Edinburgh: Earth Sciences 87, P. 43–56.

[22] Watson, E. B. and Cherniak, D. J. (1997): Oxygen diffusion in zircon. Earth and Planetary Science Letters 148, P. 527–544.

[23] Nagasawa, H. (1970): Rare earth concentrations in zircon and apatite and their host dacites and granites. Earth and Planetary Science Letters 9, P. 359–364.

[24] Watson, E. B. (1979): Zircon saturation in felsic liquids: experimental results and applications to trace element geochemistry. Contributions to Mineralogy and Petrology 70, 407–419.

[25] Murali, A. V., Parthasarathy, R., Mahadevan, T. M. and Sankar Das, M. (1983): Trace element characteristics, REE patterns and partition coefficients of zircons from different geological environments a case study on Indian zircons. Geochimica et Cosmochimica Acta 47, P. 2047–2052.

[26] Rager, H., Amthauer, G., Bernroider, M. and Schürmann, K. (1996): Color, crystal chemistry, and mineral association of a green sphalerite from Steinperf, Dill syncline, FRG. European Journal of Mineralogy: 8. P. 1191–1198.